

# Geometric Monitoring of Heterogeneous Streams

Daniel Keren, Guy Sagy, Amir Abboud, David Ben-David, Assaf Schuster, Izchak Sharfman, and Antonios Deligiannakis

**Abstract**—Interest in stream monitoring is shifting toward the distributed case. In many applications the data is high volume, dynamic, and distributed, making it infeasible to collect the distinct streams to a central node for processing. Often, the monitoring problem consists of determining whether the value of a global function, defined on the union of all streams, crossed a certain threshold. We wish to reduce communication by transforming the global monitoring to the testing of *local* constraints, checked independently at the nodes. *Geometric monitoring* (GM) proved useful for constructing such local constraints for general functions. Alas, in GM the constraints at all nodes share an identical structure and are thus unsuitable for handling heterogeneous streams. Therefore, we propose a general approach for monitoring heterogeneous streams (HGM), which defines constraints tailored to fit the data distributions at the nodes. While we prove that optimally selecting the constraints is NP-hard, we provide a practical solution, which reduces the running time by hierarchically clustering nodes with similar data distributions and then solving simpler optimization problems. We also present a method for efficiently recovering from local violations at the nodes. Experiments yield an improvement of over an order of magnitude in communication relative to GM.

**Index Terms**—Heterogeneous data streams, distributed streams, geometric monitoring, data modeling, safe zones

## 1 INTRODUCTION

FOR A few years now, processing and monitoring of distributed streams has been emerging as a major effort in data management, with dedicated systems being developed for the task [1]. This paper deals with *threshold queries* over distributed streams, which are defined as “retrieve all items  $x$  for which  $f(x) \leq T$ ”, where  $f()$  is a scoring function and  $T$  some threshold. Such queries are the building block for many algorithms, such as top- $k$  queries, anomaly detection, and system monitoring. They are also applied in important data processing and data mining tools, including feature selection, decision tree construction, association rule mining, and computing correlations. Another important application is data classification, which is often also achieved by thresholding a function, such as the output of a neural net or support vector machine.

The idea of geometric monitoring [2]–[5] has been recently proposed for monitoring such threshold queries over distributed data. While a more detailed presentation is deferred until Section 2.2, we note that geometric monitoring can be applied to the important case of scoring

functions  $f()$  evaluated at the average (weighted average is handled in a similar way) of dynamic data vectors  $v_1(t), \dots, v_n(t)$ , maintained at  $n$  distributed nodes. Here,  $v_i(t)$  is an  $m$ -dimensional data vector, often denoted as *local vector*, at the  $i$ -th node  $N_i$  at time  $t$  (often  $t$  will be omitted for brevity). In a nutshell, each node monitors a convex subset, often referred to as the node’s *safe-zone*, of the *domain* of these data vectors, as opposed to their *range*. What is guaranteed in the geometric monitoring approach is that the global function  $f()$  will not cross its specified threshold as long as all data vectors lie within their corresponding safe-zones. Thus, each node remains silent as long as its data vector lies within its safe zone. Otherwise, in case of a safe-zone breach, communication needs to take place in order to check if the function has truly crossed the given threshold.

The geometric technique can support any scoring function  $f()$ , evaluated at the average of the dynamic data vectors. Thus,  $f()$  is not assumed to obey some simple property (e.g., linearity or monotonicity). To add to the generality of the technique [3], [6], there is absolutely no requirement that the  $v_i$  data vectors simply consist of the raw data/measurements of the distributed nodes – in fact, a component of a  $v_i$  vector can be either raw data, or any function (i.e., norm, logarithm, power, variance, etc) computed over the data of  $N_i$ . Thus, geometric monitoring allows the monitoring of functions that are far more complex and general than simple aggregates. Examples of diverse and important supported functions are:

- D. Keren is with the Department of Computer Science, Haifa University, Haifa 31905, Israel. E-mail: dkeren@cs.haifa.ac.il.
- G. Sagy, A. Abboud, D. Ben-David, A. Schuster, and I. Sharfman are with the Faculty of Computer Science, Israeli Institute of Technology, Haifa 31905, Israel. E-mail: {guysagy, amir.abboud, sdavidbd, tsachis}@gmail.com; assaf@cs.technion.ac.il.
- A. Deligiannakis is with the Department of Electronic and Computer Engineering, Technical University of Crete, Chania 73100, Greece. E-mail: adeli76@yahoo.com.

Manuscript received 16 June 2013; revised 6 Nov. 2013; accepted 10 Nov. 2013. Date of publication 4 Dec. 2013; date of current version 10 July 2014. Recommended for acceptance by G. Cormode.  
For information on obtaining reprints of this article, please send e-mail to: reprints@ieee.org, and reference the Digital Object Identifier below.  
Digital Object Identifier 10.1109/TKDE.2013.180

- Correlation monitoring [2]: Documents may be classified based on the features in them. The local vectors  $v_i$  are the contingency tables of e.g. document class

- vs. feature, and  $f()$ , evaluated at the average (global) contingency table, is the correlation coefficient or chi-square.
- The analysis of *frequency moments* [7] over distributed data streams, in which a global function is monitored over the average of the streams. Here  $v_i$  are typically local histograms and  $f()$  the  $L^p$  norm for some  $p$ .
- The system monitoring paradigm described in [8]: the  $v_i$  are scatter matrices constructed at each node, and  $f()$  is computed from the eigenvalues of the average matrix.
- Monitoring various measures (i.e.,  $L^p$  norms, cosine similarity, Extended Jaccard Coefficient, correlation coefficient) for detecting outliers in sensor networks [3].

A crucial component for reducing the communication required by the geometric method is the design of the safe-zone in each node. Nodes remain silent as long as their local vectors remain within their safe-zone. Thus, good safe-zones increase the probability that nodes will remain silent, while also guaranteeing correctness: a global threshold violation cannot occur unless at least one node's local vector lies outside the corresponding node's safe-zone.

However, prior work on geometric monitoring has failed to take into account the nature of heterogeneous data streams, in which the data distribution of the local vectors at different nodes may vary significantly. This has led to a uniform treatment of all nodes, independently of their characteristics, and the assignment of identical safe-zones (i.e., of the same shape and size) to all nodes.

As we demonstrate here, designing safe-zones that take into account the data distribution of nodes can lead to efficiently monitoring threshold queries at a fraction (requiring an order of magnitude fewer messages) of what prior techniques achieve. However, designing different safe-zones for the nodes is by no means easy. In fact, we demonstrate that this problem is not only NP-hard, but also inapproximable. We, thus, propose a more practical solution that hierarchically clusters nodes, based on the similarity of their data distributions, and then seeks to solve many small (and easier) optimization problems. We demonstrate that the proposed solution scales significantly better than the optimal algorithm, while resulting in only a marginal decrease in the quality of the obtained solution. We emphasize that the optimization algorithm which computes the individual safe-zones is actually performed infrequently, since there is no need to modify the safe-zone of a node unless the value of the function actually crosses the threshold. While the main goal of our algorithms is to reduce communication by minimizing the number of safe-zone breaches by the local vectors (we refer to such breaches as *local violations*), we also propose a method for efficiently recovering from local violations, by carefully picking the nodes to communicate with. The contributions of this work are:

- We formulate a far more general safe-zone assignment problem than those which were treated so far. Instead of constructing one safe-zone which is common to all nodes, we seek to fit each node with a safe-zone that suits its data distribution.

- We study the complexity of this general problem and prove that it is NP-hard and inapproximable.
- We present a practical solution, which uses hierarchical clustering of the nodes to construct the safe-zones, while applying various geometric and computational tools.
- We present an algorithm for efficiently recovering from safe-zone breaches.
- The resulting safe-zones were tested on real data, where we demonstrate that: (i) the hierarchical clustering approach dramatically reduces the running time requirements, compared to an optimal algorithm, with only a marginal decrease in the quality (target function) of the obtained solution, (ii) our techniques may result in one order of magnitude (or even larger) improvements in communication over previous geometric monitoring methods, even for a small number of nodes, and (iii) our algorithm for recovering from safe-zone breaches manages to resolve them by requesting the data (on average) of few nodes.

**Outline.** We survey related work in Section 2. In Section 3 we formulate our optimization problem, which involves the design of safe-zones at the nodes. Section 4 presents our algorithmic framework. In Section 5 an algorithm for recovery from a safe-zone violation is discussed. Experiments are resented in Section 6. In Section 7 we prove that the newly presented problem of optimal safe-zone assignment is NP-hard. Conclusions are provided in Section 8.

We, hereafter, denote our proposed method for geometric monitoring of heterogeneous streams as **HGM**, in contrast to prior work on geometric monitoring that is denoted as **GM**.

## 2 RELATED WORK

### 2.1 Distributed Monitoring and Summarization Techniques

Previous methods for reducing communication in distributed systems include *sketching*, [7], [9], [10]. Other research concerns detecting "heavy hitters" [11], [12], computing quantiles [13], counting distinct elements [14], optimal sampling [15], distributed monitoring of decision trees [16], and ranking [17]. Theoretical analysis of the monitoring problem is provided in [18], and some non-monotonic functions of frequency moments are treated in [19]. The BBQ system [20] constructs a dynamic probabilistic model for the collection of sensor measurements. The system determines whether it is possible to answer queries only given the model values, or whether it is necessary to poll some of the sensors. In [21], data uncertainty in monitoring linear queries over distributed data is handled by fitting the data with a probabilistic model and devising an optimal monitoring scheme with respect to this model.

A great deal of work [22] exists for the case in which the threshold function is *linear* (e.g., aggregate, average). However, many functions of interest are *non-linear* and *non-monotonic* and, as elaborated in past work (e.g., [2]), pose a formidable problem for monitoring tasks, whose solution requires a radically different approach than those used for linear/monotonic functions. applies a distributed paradigm

TABLE 1  
Glossary of Common Notations

$N_1, \dots, N_n$	$n$ distributed nodes with a central coordinator.	$C$	A convex subset of $A$ , defined as in previous work [5].
$v_i(t)$ (or $v_i$ )	Dynamic data vector at node $N_i$ .	$p_i$	Probability distribution function (pdf) at node $N_i$ .
$v(t)$ (or $v$ )	The average of the $v_i$ vectors.	$S_i$	Safe-zone at node $N_i$ .
$f()$	The monitored function.	GM	Previous geometric monitoring methods.
HGM	The proposed approach for geometric monitoring of heterogeneous streams.	$T$	Threshold: the monitored condition is $f(v) \leq T$ .
$A$	The admissible region, defined as all $v$ such that $f(v) \leq T$ .	Local violation global violation	When $v_i \notin S_i$ When $v \notin C$

to decide on the dimension of an approximating subspace for distributed data, with the application of detecting system anomalies such as a DDoS attack. A theoretical paper discussed functional approximation in a distributed setting [18], but it only deals with obtaining lower and upper bounds for vector norm functions. This is also studied in [23], in which moment-based functions and the “distinct item count” problem are addressed. In [24] an algorithm is provided for determining whether the norm of the average vector in a distributed system is below a certain threshold, or more generally, whether it lies inside some convex set; however, it does not deal with general functions. In [25] the value of a polynomial in one variable is monitored. A great deal of work was dedicated to distributed monitoring of monotonic functions, usually weighted averages, *max* and *min* operators etc. [26]. Querying non-monotonic functions by representing them as a difference of monotonic ones is presented in [6], but for a static database. Ratio queries over streams are treated in [27], based on a dynamic model which monitors the local ratios vis-a-vis optimally chosen local thresholds. We also handle ratio queries, but in a different method, which is based on optimizing with respect to the data distribution at the nodes. The work in [27] does handle the case of issuing an alert if the ratio of two aggregated (over time) dynamic variables crosses a certain threshold, but does not naturally extend to handle instantaneous (based only on the current values) ratios, such as the ones that we target in our experiments.

## 2.2 Geometric Monitoring

We now describe some basic ideas regarding the geometric monitoring (GM) technique, which was introduced and applied to monitor distributed data streams in [2], [28]. Table 1 summarizes some important notation.

As described in Section 1, each node  $N_i$  maintains a local vector  $v_i$ , while the monitoring function  $f()$  is evaluated at the average  $v$  of the  $v_i$  vectors. Before the monitoring process, each node  $N_i$  is assigned a subset of the data space, denoted as  $S_i$  – its *safe-zone* – such that, as long

as the local vectors are inside their respective safe-zones, it is guaranteed that the global function’s value did not cross the threshold; thus the node remains silent as long as its local vector  $v_i$  is inside  $S_i$ . For details and scope see [5] and the survey in [29]. Recently, GM was successfully applied to detecting outliers in sensor networks [3], extended to prediction-based monitoring [4], and applied to other monitoring problems [30]–[32].

A basic construct in GM is the *admissible region*, defined by  $A \triangleq \{v | f(v) \leq T\}$ . Since the value we wish to monitor is  $f(\frac{v_1 + \dots + v_n}{n})$ , any viable assignment of safe-zones must satisfy  $\bigwedge_{i=1}^n (v_i \in S_i) \rightarrow v = \frac{v_1 + \dots + v_n}{n} \in A$ . This guarantees that as long as all nodes are silent, the average of the  $v_i$  vectors remains in  $A$  and, therefore, the function has not crossed the threshold. In case of a local violation (safe-zone breach) communication needs to take place in order to check if the function has truly crossed the given threshold. This process may naively always require the collection of the  $v_i$  vectors from all nodes, or it can be performed more efficiently using our violation recovery algorithm, described in Section 5. The question is, of course, how to determine the safe-zone  $S_i$  of each node  $N_i$ ; in a sense to be made precise in Section 3, it is desirable for the safe-zones to be as large as possible.

In [5] it was proved that all existing variants of GM share the following property: each of them defines some convex subset  $C$  of  $A$  (different methods induce different  $C$ ’s), such that each safe-zone  $S_i$  is a translation of  $C$  (see Fig. 1)—that is, there exist vectors  $u_i$  ( $1 \leq i \leq n$ ) such that  $S_i = \{u_i + c | c \in C\}$  and  $\sum_{i=1}^n u_i = 0$ .

This observation unifies the distinct variants of GM, and also allows to easily see why  $\bigwedge_{i=1}^n (v_i \in S_i)$  implies that  $v = \frac{v_1 + \dots + v_n}{n} \in C \subseteq A$  – it follows immediately from the fact that convex subsets are closed under taking averages and from the fact that the  $u_i$  vectors sum to zero. Methods for constructing  $C$  include:

- The method of *bounding spheres* [2]. A point  $p \in A$  (the “reference point”) is defined to be the average of the vectors  $v_i(0)$ , and  $C$  is defined as the set of

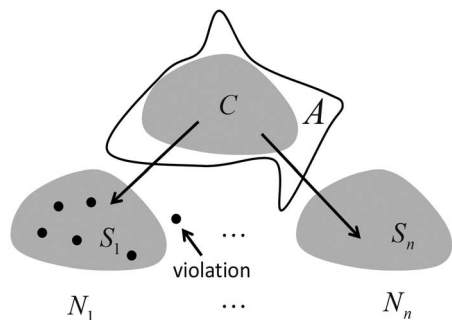


Fig. 1. Schematic description of the GM method. A convex subset  $C$  of the admissible region  $A$  is determined, and then each node  $N_k$  is assigned a safe-zone which is a translation of  $C$ .

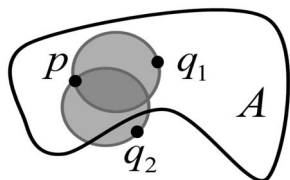


Fig. 2. ‘‘Bounding spheres’’ approach. The point  $q_1$  belongs to  $C$ , since the ball whose diameter is the segment  $\overline{pq_1}$  is contained in  $A$ ; however,  $q_2$  does not belong to  $C$ , as the corresponding ball is not contained in  $A$ .

all points  $q$  such that the ball whose diameter is the segment  $\overline{pq}$  is entirely contained in  $A$  (see Fig. 2).

- ‘‘Shape sensitive geometric monitoring’’ [5], [28]. In this approach the bounding spheres algorithm was improved by a better choice of the reference point  $p$ , as well as replacing the bounding spheres by ellipsoids whose parameters approximate the distribution of the data at the nodes (but with the underlying assumption that this distribution is shared by all nodes).
- The ‘‘optimized safe-zones’’ approach, briefly introduced in [5], consists of searching for a subset  $C$  of  $A$  which is both convex and ‘‘good’’, in the sense that  $\int_C p(v)dv$  is large, where  $p(v)$  is the probability density function (termed as pdf hereafter) of the data distribution. The motivation is straightforward – as the integral becomes larger, then on the average it will take the data vectors more time to exit  $C$ .

In this paper we assume that  $C$  is given; it can be provided by any of the abovementioned methods (obviously, if  $A$  itself is convex, we just choose  $C = A$ ). We propose to extend previous work in a more general direction. Our goal here is to handle a basic problem which haunts all the existing GM variants: *the shapes of the safe-zones at different nodes are identical*. Thus, if the data is heterogeneous across the distinct streams (an example is depicted in Fig. 3), meaning that the data at different nodes obeys different distributions, existing GM algorithms will perform poorly, causing many local violations that do not correspond to global threshold crossing (false alarms).

In this paper, we present a more general approach that allows to assign *differently shaped* safe-zones to different nodes. As we will shortly demonstrate, our approach requires tackling a difficult optimization problem, for which practical solutions need to be devised.

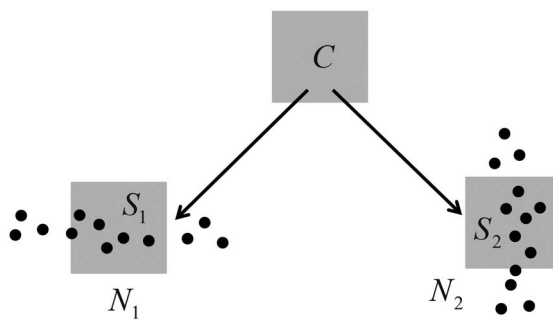


Fig. 3. Why GM may fail for heterogeneous streams. Here  $C$  is equal to a square, and the data distribution at the two nodes is schematically represented by samples. In GM, the safe-zones at both nodes are restricted to be a translation of  $C$ , and thus cannot cover the data; HGM will allow much better safe-zones (see Section 3, Fig. 4).

### 3 SAFE-ZONE DESIGN AS AN OPTIMIZATION PROBLEM

We now seek to formulate an optimization problem, whose output is the safe-zones at all nodes. The safe-zones should satisfy the following properties:

**Correctness:** If  $S_i$  denotes the safe-zone at node  $N_i$ , we must have:

$\bigwedge_{i=1}^n (v_i \in S_i) \rightarrow \frac{v_1 + \dots + v_n}{n} \in C$ . This ensures that every threshold crossing by  $f(v)$  will result in a safe-zone breach in at least one node, that is, *all* global violations are captured.

**Expansiveness:** Every safe-zone breach (local violation) triggers communication, so the safe-zones should be as ‘‘large’’ as possible. We measure the ‘‘size’’ of a safe-zone  $S_i$  by its probability volume, defined as  $\int_{S_i} p_i(v)dv$  where

$p_i$  is the pdf of the data at node  $N_i$ . Probabilistic models have proved useful in predicting missing and future stream values in various monitoring and processing tasks [20], [21], [33], including previous geometric methods [5], and their incorporation in our algorithms proved useful in monitoring real data (Section 6).

**Simplicity:** At each time step, every node must check whether its data vector is in its safe-zone. To render this task computationally feasible (especially for thin nodes, such as sensors) it is desirable that the safe-zones be simple geometric constructs. The simplicity of the safe-zones is governed by the user, as he/she defines the family of shapes to which the safe-zones belong (Sections 4.2, 6.1.2).

To handle the correctness and expansiveness requirements, we formulate a constrained optimization problem as follows:

**Given:** (1) probability distribution functions  $p_1, \dots, p_n$  at  $n$  nodes  
 (2) A convex subset  $C$  of the admissible region  $A$

Maximize  $\int_{S_1} p_1 dv_1 \dots \int_{S_n} p_n dv_n$  (expansiveness)

Subject to  $\frac{S_1 \oplus \dots \oplus S_n}{n} \subseteq C$  (correctness)

where  $\frac{S_1 \oplus \dots \oplus S_n}{n} = \left\{ \frac{v_1 + \dots + v_n}{n} \mid v_1 \in S_1, \dots, v_n \in S_n \right\}$ , or the *Minkowski sum* [34] of  $S_1, \dots, S_n$ , in which every element is divided by  $n$  (the *Minkowski average*). Introducing the

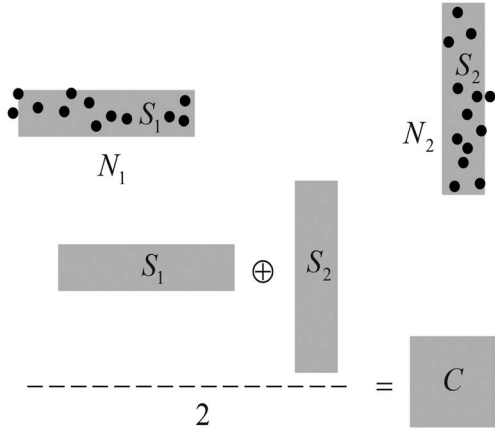


Fig. 4. Schematic example of HGM safe-zone assignment for two nodes, which also demonstrates the advantage over previous work. The convex set  $C$  is a square, and the pdf at the left (right) node is uniform over a rectangle elongated along the horizontal (vertical) direction. HGM can handle this case by assigning the two rectangles  $S_1, S_2$  as safe-zones, which satisfies the correctness requirement (since their Minkowski average is equal to  $C$ ). GM (Fig. 3) will perform poorly in this case.

Minkowski average is necessary in order to guarantee correctness, since  $v_i$  must be able to range over the entire safe-zone  $S_i$ . Note that instead of using the constraint  $\frac{S_1 \oplus \dots \oplus S_n}{n} \subseteq A$ , we use  $\frac{S_1 \oplus \dots \oplus S_n}{n} \subseteq C$ . This preserves correctness, since  $C \subseteq A$ . The reason we chose to use  $C$  is that, as it turns out, typically it's much easier to check the constraint for the Minkowski average containment in a convex set; this is discussed in Section 4.4.

To derive the target function  $\int_{S_1} p_1 dv_1 \cdot \dots \cdot \int_{S_n} p_n dv_n$ , which estimates the probability that the local vectors of all nodes will remain in their safe-zones, we assumed that the data is not correlated between nodes, as it was the case in the experiments in Section 6 (see also [21] and the discussion therein). If the data is correlated, the algorithm is essentially the same, with the expression for the probability that data at some node breaches its safe-zone modified accordingly. We plan to target such cases in the future.

Note that correctness and expansiveness have to reach a "compromise": figuratively speaking, the correctness constraint restricts the size of the safe-zones, while the probability volume increases as the safe-zones become larger. This trade-off is central in the solution of the optimization problem.

The advantage of the resulting safe-zones is demonstrated by a schematic example (Fig. 4), in which  $C$  and the stream pdfs are identical to those in Fig. 3. In HGM, however, the individual safe-zones can be shaped very differently from  $C$ , allowing a much better coverage of the pdfs, while adhering to the correctness constraint. Intuitively speaking, nodes can trade "geometric slack" between them; here  $S_1$  trades "vertical slack" for "horizontal slack".

**The Complexity of the Safe-Zone Problem.** The input to the safe-zone problem consists of  $C$  and the probability distributions  $p_i$ . The difficulty of the problem increases with the number of nodes, the dimensionality of the data, and the complexity of the  $p_i$ s. In Section 7 we prove that the

problem is NP-hard and inapproximable. In the next section, we thus seek to devise practical algorithms to solve this problem.

## 4 CONSTRUCTING THE SAFE-ZONES

We now briefly describe the overall operation of the distributed nodes. The computation of the safe-zones is initially performed by a coordinator node, using a process described in this section. This process is performed infrequently, since there is no need to modify the safe-zone of a node unless a global threshold violation occurs. As described in Section 3, the input to the algorithm is: (1) The probability distribution functions  $p_1, \dots, p_n$  at the  $n$  nodes. These pdfs can be of any kind (e.g., Gaussian [28], random walk [25], uniform, etc). Moreover, these pdfs may be given either analytically or by a sample. As discussed in Section 4.5, message passing between the nodes and the coordinator in this initial phase can be reduced by using compact data representations; (2) A convex subset  $C$  of the admissible region  $A$ .

After the individual safe-zones have been computed, they are assigned to each node. This process is the end of the *initialization stage*. Each node  $N_k$  does not initiate communication as long as  $v_k(t) \in S_k$ . If  $v_k(t) \notin S_k$  (local violation) the algorithm described in Section 5 is applied to try and resolve the violation.

### 4.1 Solving the Optimization Problem

In order to efficiently solve our optimization problem, we need to answer several questions:

- What kinds of shapes to consider for candidate safe-zones? This is discussed in Section 4.2.
- The target function is defined as the product of integrals of the respective pdfs on the candidate safe-zones. Given candidate safe-zones, how do we efficiently compute the target function? This is discussed in Section 4.3.
- Given candidate safe-zones, how do we efficiently test if their Minkowski average lies in  $C$ ? This is discussed in Section 4.4.
- As we will point out, the number of variables to optimize over is very large, with this number increasing with the number of nodes. It is well-known that the computational cost of general optimization routines increases at a super-linear rate with the number of variables. To remedy this issue, we propose in Section 4.5 a hierarchical clustering approach, which uses a divide-and-conquer algorithm to reduce the problem to that of recursively computing safe-zones for small numbers of nodes.

### 4.2 Shape of Safe-Zones to Consider

The first step in solving an optimization problem is determining the parameters to optimize over. Here, the space of parameters is huge – *all* subsets of the Euclidean space are candidates for safe-zones. The space of all subsets is extremely complicated: not only is it infinite-dimensional, but also non-linear [35]. For one-dimensional (scalar) data,

intervals provide a reasonable choice for safe-zones, but for higher dimensions no clear candidate exists.

To achieve a practical solution, we choose the safe-zones from a parametric family of shapes, denoted by  $S$ . This family of shapes should satisfy the following requirements:

- It should be broad enough so that its members can reasonably approximate every subset which is a viable candidate for a safe-zone. If this does not hold, the solution may be grossly sub-optimal. This point is discussed and explained in Section 6.1.2.
- The members of  $S$  should have a relatively simple shape (the “simplicity” property, Section 3). In practice, this means that they are polytopes with a restricted number of vertices, or can be defined by a small number of implicit equations (e.g., polynomials [36]). See further discussion in Section 6.1.2.
- It should not be too difficult to compute the integral of the various pdfs over members of  $S$  (Section 4.3).
- It should not be too difficult to compute, or bound, the Minkowski average of members of  $S$  (Section 4.4).

The last two conditions allow efficient optimization. If computing the integrals of the pdf or the Minkowski average are time consuming, the optimization process may be lengthy. We thus considered and applied in our algorithms various polytopes (such as triangles, boxes, or more general polytopes) as safe-zones, a choice which yielded good results for the simpler problem in [5].

As explained in the experimental evaluation (see discussion in Section 6.1.2), this choice depends on the function  $f()$ . However, the challenge of choosing the best shape for arbitrary functions and data distributions is, by itself, quite formidable; we now elaborate on a very general paradigm to obtain a good choice.

**Bayesian model selection.** We propose to view the problem of choosing the family of safe-zones to optimize over as an instance of the *model selection* problem. Very often, it is required to fit a model (e.g. a polynomial approximation) to data. This model is chosen from a graded family of models of increasing complexity and descriptive power: for polynomials the models are ordered by their degree, in our case the safe-zones are ordered by the number of their vertices. One must choose the sub-family of the model to be used (e.g. the degree of the polynomial or the number of safe-zone vertices). The optimal choice achieves a tradeoff between the approximation quality of the model and the number of its parameters; obviously, the approximation quality increases with the number of parameters, but eventually it is “saturated”, meaning that adding more parameters hardly affects the quality, leads to overfitting, and violates the “simplicity of the safe-zone” demand (Section 3). To obtain the optimal choice, we have applied *Bayesian model selection* [37], [38]. Space does not permit to survey the derivations, so we will just provide the result:

**Lemma 1.** *For any natural number  $m$ , denote by  $F_m$  the solution of the safe-zone assignment problem which applies polytopes with  $m$  vertices, and denote the value of the target function by  $E_m$ . The optimal model is the one which maximizes  $\log(E_m) + c|H_m|^{\frac{1}{2}}$ , where  $H_m$  is the Hessian matrix of the solution parameters, and  $c$  a constant which depends*

*only on the dimension of the data vectors. The expression  $\log(E_m) + c|H_m|^{\frac{1}{2}}$  is referred to as the **model evidence**.*

The practical meaning of this criterion is the following: as  $m$  increases, we obtain a better approximation of the pdf’s at the nodes, hence  $\log(E_m)$  increases. However, since the safe-zones will eventually “saturate” the pdf’s (meaning that increasing  $m$  only slightly increases the target function), the optimal fit becomes very “flat” in parameter space, hence the determinant of the Hessian will become very small. Bayesian model selection thus provides a rigorous choice of a model which obtains the optimal tradeoff between the quality of the model and the number of parameters. To quickly find the optimal  $m$ , binary search can be applied.

In the experiments (Section 6) we applied both Bayesian model selection and simple safe-zones (triangles and boxes), for monitoring non-linear, non-monotonic functions.

**A note on the complexity of the problem.** The optimization problem we must solve to obtain the safe-zones is quite more demanding than that in [5], which uses the same safe-zone for each node. For example, suppose that the data vectors are two-dimensional, there are 100 nodes, and we apply octagonal safe-zones. The optimization problem in [5] requires optimizing over 16 parameters (8 vertices for the single octagonal safe-zone common to all nodes, with each vertex having two coordinates), but for the general case treated here, an octagonal region should be defined for every node, yielding a total of 1,600 parameters. Further, the Minkowski sum constraint,  $\frac{S_1 \oplus \dots \oplus S_n}{n} \subseteq C$ , introduces a coupling between the parameters, making it impossible to separate the optimization problem into disjoint problems with a smaller number of parameters. No simple solution to this problem exists, since it is NP-hard and inapproximable (Section 7).

### 4.3 Computing the Target Function

The target function is defined as the product of integrals of the respective pdfs on the candidate safe-zones. Typically, data is provided as discrete samples. The integral can be computed by first approximating the discrete samples by a continuous pdf, and then integrating it over the safe-zone. We used this approach, fitting a GMM (Gaussian Mixture Model) to the discrete data and integrating it over the safe-zones, which were defined as polytopes. To accelerate the computation of the integral, we used Green’s Theorem to reduce a double integral to a one-dimensional integral over the polygon’s boundary: the integral of a general two-dimensional Gaussian in  $x, y$ ,  $\exp(- (A^2 + Bxy + C^2 + Dx + Ey + F))$  over a region  $R$  equals the integral of  $\frac{\sqrt{\pi}}{2\sqrt{A}} \exp\left(-\left(Ey + Cy^2 + F - \frac{(D+By)^2}{4A}\right)\right) \operatorname{erf}\left(\sqrt{A}x + \frac{D+By}{2\sqrt{A}}\right)$  over  $R$ ’s boundary. For higher dimensions, the integral can also be reduced to integrals of lower dimensions, or computed using Monte-Carlo methods.

### 4.4 Checking the Constraints

**The Half-Planes Method.** To implement a constrained optimization routine, a function is required which checks whether the current parameters satisfy the constraints. This function should return zero if the constraints are satisfied, and a positive number if not. It should also behave

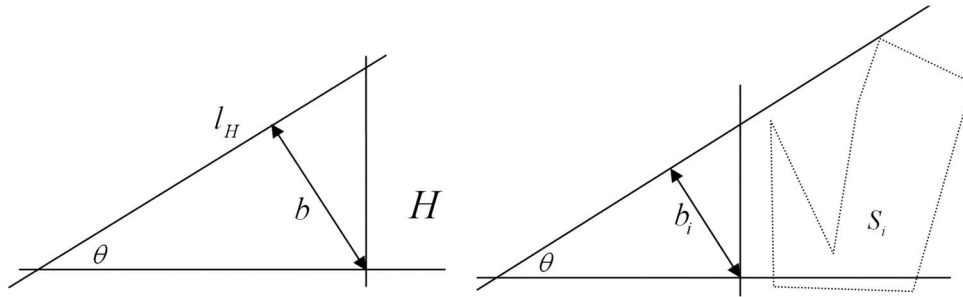


Fig. 5. Half-plane approach, for  $C$  equal to  $H$  which is defined by  $\theta$  and  $b$  (left), by using a supporting hyper-plane for every safe-zone candidate  $S_i$  (right).

smoothly – if the constraint violation is small, it should return a small value.

In our case, the constraint is that the Minkowski average of the safe-zones is contained in  $C$ . One way to check the constraint is to compute the Minkowski average and test whether it is inside  $C$  and, if not, determine some measure of its deviation from  $C$ . Alas, this may entail very high computational complexity, especially in high dimensions, in which computing the Minkowski sum is computationally extensive [39]. To overcome this, we used the following method, which allows to test the constraint without explicitly computing the Minkowski average. For the sake of simplicity we explain the solution for two-dimensional data, but the algorithm proceeds similarly in every dimension. We start with the simple case, in which  $C$  is a half-plane (Fig. 5), denoted  $H$ , and then generalize. Denote the half-plane's boundary by  $l_H$ , so  $H$  is the set of points below  $l_H$  (the algorithm proceeds similarly if  $l_H$  is  $H$ 's lower boundary). The line  $l_H$  is defined by the angle  $\theta$  and by  $b$ , its distance from the origin (in higher dimensions similar definitions hold, with the direction of the  $b$  vector replaced by a unit vector perpendicular to the hyperplane). Then, in order to determine whether the Minkowski average of the candidate safe-zones  $S_1, \dots, S_n$  is contained in  $H$ , one has to find for each  $S_i$  the upper supporting line (in higher dimensions, upper supporting hyperplane) in the same direction as that of  $l_H$ . For a polytope  $S_i$ , this requires rather low computational complexity – only the vertices need to be considered and line sweep algorithms can be applied to further reduce running time. In order for the Minkowski average of the  $S_i$ 's to be contained in  $H$ , it is sufficient that  $\frac{\sum b_i}{n} \leq b$ . This algorithm also allows to measure the amount of constraint violation, which depends on the value of  $\frac{\sum b_i}{n} - b$ .

If  $C$  is a convex polytope, then  $C$  is equal to the intersection of half-planes, and the measure of constraint violation is defined as the max (using the sum is also plausible) of the measures corresponding to the individual half-planes. A general convex  $C$  can be efficiently approximated by an inscribed convex polytope [40]. Alternatively, the following method can be used.

**The Direct Method.** A more direct method to test the Minkowski sum constraint relies on the following result [41]:

**Lemma 2.** *If  $P$  and  $Q$  are convex polytopes with vertices  $\{P_i\}, \{Q_j\}$ , then  $P \oplus Q$  is equal to the convex hull of the set  $\{P_i + Q_j\}$ .*

Now, assume we wish to test whether the Minkowski average of  $P$  and  $Q$  is contained in  $C$ . Since  $C$  is convex, it contains the convex hull of every of its subsets; hence it suffices to test whether the points  $(P_i + Q_j)/2$  are in  $C$ , for all  $i, j$ . If not all points are inside  $C$ , then the constraint violation can be measured by the maximal distance of a point  $(P_i + Q_j)/2$  from  $C$ 's boundary. The method easily generalizes to more polytopes: for three polytopes it is required to test the average of all triplets of vertices, etc.

#### Comparison of the Half-Planes and Direct Methods.

Assume candidate safe-zones  $S_1, \dots, S_n$ , where  $S_i$  has  $V(S_i)$  vertices. Since in the half-planes method the position of every half-plane vs. every summand is computed separately, the running time is proportional to  $H_C \sum_{i=1}^n V(S_i)$ , where  $H_C$  is the number of half-planes defining  $C$ . The running time of the direct method is proportional to  $t_C \prod_{i=1}^n V(S_i)$ , where  $t_C$  is the time required for checking if a point is inside  $C$ . Given the types of the candidate safe-zones, their number, and the definition of  $C$ , one can choose the method with the lower computational complexity. For example, when many nodes are present, the half-planes method will usually do better. If  $C$  is defined by an implicit equation  $g()$  (e.g., an ellipsoid) then testing for the presence of a point  $v$  in  $C$  is easy (i.e.,  $v \in C$  iff  $g(v) \leq 0$ ), and the direct method is then better (unless  $\prod_{i=1}^n V(S_i)$  is large enough to offset this advantage). In Section 6 some examples are given as to how these considerations are applied.

#### 4.5 Hierarchical Clustering

While the algorithms presented in Sections 4.3-4.4 reduce the running time for computing the safe-zones, our optimization problem still poses a formidable difficulty. For example, as discussed in Section 4.2, fitting octagonal safe-zones to 100 nodes with two-dimensional data requires to optimize over 1,600 variables, which is quite high for a general optimization problem. To alleviate this problem, we first organize the nodes in a hierarchical structure, which allows us to then solve the problem recursively (top-down in this hierarchical structure) by reducing it to sub-problems, each containing a much smaller number of nodes.

We first perform a bottom-up hierarchical clustering of the nodes. To achieve this, a distance measure between nodes needs to be defined. Since a node is represented by its data vectors, a distance measure should be defined between

subsets of the Euclidean space. We apply the method in [42], which defines the distance between sets by the  $L^2$  distance between their moment vectors (vectors whose coordinates are low-order moments of the set). The moments have to be computed only once, in the initialization stage. The leaves of the cluster tree are individual nodes, and the inner vertices can be thought of as “super nodes”, each containing the union (Minkowski average) of the data of nodes in the respective sub-tree. Since the moments of a union of sets are simply the sum of the individual sets’ moments, the computation of the moment vectors for the inner nodes is very fast.

After the hierarchical clustering is completed, the safe-zones are assigned top-down: first, the children of the root are assigned safe-zones under the constraint that their Minkowski average is contained in  $C^1$ . In the next level, the grandchildren of the root are assigned safe-zones under the constraint that their Minkowski average is contained in their parent nodes’ safe-zones, etc. The leaves are either individual nodes, or clusters which are uniform enough and can all be assigned safe-zones with identical shapes.

**Reducing the Transmitted Parameters.** Data should be sent from the nodes to the coordinator in order to allow computing the safe-zones, and the coordinator has to send the nodes the definition of their safe-zones. In our experiments this was achieved not by passing the entire data, but the far more compact parameters of the pdf and the first and second order moments of the data, which suffice to compute the safe-zones. If the data at the nodes is very large, we may use a sample to compute its moments. Sending the safe-zone parameters to the nodes is also very fast, as the safe-zones are described by a relatively small number of parameters.

## 5 VIOLATION RECOVERY

Recall that we define a *local violation* at time  $t$  at  $N_i$  if its local vector  $v_i(t)$  wandered out of its safe-zone  $S_i$ . A *global violation* occurs when the average of the vectors in all nodes exits  $C$ . Clearly, a global violation implies at least one local violation, however the opposite may not be true, in which case the local violation constitutes a *false alarm*, which should be detected as such and resolved with minimal communication. Often, a different node can remedy the violation: assume that the current local vector  $v_j(t)$  at  $N_j$  satisfies  $v_i(t) + v_j(t) \in S_i \oplus S_j$ . Then,  $N_i$  and  $N_j$  “balance” each other and the local violation is resolved with minimal communication overhead (the only communication is between nodes  $N_i$  and  $N_j$ , either directly or through the coordinator). In previous work [2], [28] the coordinator randomly chose nodes in an attempt to balance local violations. Here, we present a more rigorous and efficient method, based on partitioning the collection of nodes to disjoint pairs which optimally balance each other. This proceeds as follows: denoting the data set of node  $N_i$  by  $D_i$ , define a non-directed, weighted, complete graph over the nodes with the weight of the edge connecting  $N_i$  and  $N_j$  given by  $w(i, j) = \Pr(x_i + x_j \in S_i \oplus S_j) | x_i \in D_i \wedge x_j \in D_j$ . These weights are all computed at the coordinator. Please

1. This proceeds using the same algorithms described in Sections 4.3-4.4

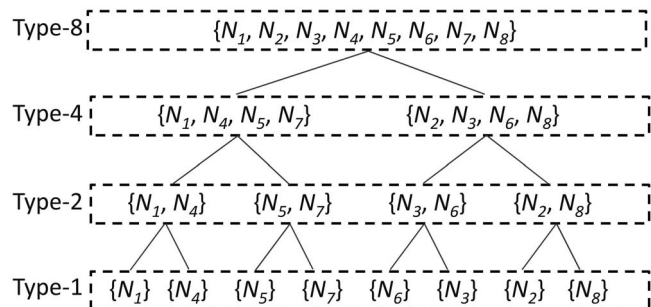


Fig. 6. Conceptual hierarchy of nodes used for violation recovery. Depicting the Type- $k$  neighbors for a sample network of 8 nodes.

note that  $w(i, j)$  can also be computed from the pdfs of the nodes, transmitted to the coordinator in a compact manner, as described at the end of Section 4.5. Then, perform a maximal perfect matching in this graph. The weight of an edge between two nodes is defined as the percentage of pairs of data vectors from both nodes whose sum is in the Minkowski sum of the nodes’ safe-zones; therefore, the larger the weight, the higher the probability that the two nodes will balance each other. This matching partitions the nodes into *disjoint* pairs which have an overall high probability to resolve each other’s local violations. Please note that if every node  $N_i$  simply attempts to balance with node  $N_j$  such that  $w(i, j)$  is maximal, the system may quickly run into deadlock when many nodes try to balance with the same node – this cannot happen with a disjoint partition.

To handle cases in which the optimal pairing fails to resolve the violation, a hierarchical structure, somewhat resembling the one used for hierarchical clustering, is applied to generalize the disjoint pairing. Following the optimal pairing of nodes, each pair is viewed as a single node whose data is the union of the data at both nodes, and maximal perfect matching is performed on the resulting graph (which has half the number of vertices as the original graph). This process is continued, with the nodes of the next graph corresponding to quadruples of nodes, etc. Call the original nodes “Type 1 node”, the pairs obtained in the first maximal perfect matching “Type 2 nodes”, the nodes corresponding to quadruples “Type 4 nodes” etc. When the safe-zone at a Type 1 node (i.e., node  $N_i$ ) is breached, the coordinator attempts to resolve the violation with  $N_i$ ’s partner in the Type 2 node it belongs to. If unsuccessful, it attempts to resolve the violation with the nodes that belong in the subtree of its partner in the Type 4 node it belongs to: if the Type 4 node containing  $N_i$  also contains nodes  $N_j, N_k, N_l$ , the violation is resolved if  $v_i(t) + v_j(t) + v_k(t) + v_l(t) \in S_i \oplus S_j \oplus S_k \oplus S_l$ , etc. The overall operation requires  $\log(n)$  rounds in the worst case, which helps bound its latency.

Fig. 6 demonstrates a scenario with 8 nodes. We explain two cases: (1)  $N_7$  is the only node with a local violation. Then, the coordinator requests the local vector from node  $N_5$ . If the violation is not resolved, it asks the local vectors from  $N_1$  and  $N_4$ , etc. (2)  $N_7$  and  $N_1$  exhibit local violations. Then, the local vectors from  $N_7$  and  $N_1$  are transmitted to the coordinator, which can then examine whether these two nodes balance each other. If not, it requests the data of their Type 2 neighbors, namely from nodes  $N_5$  and  $N_4$ .

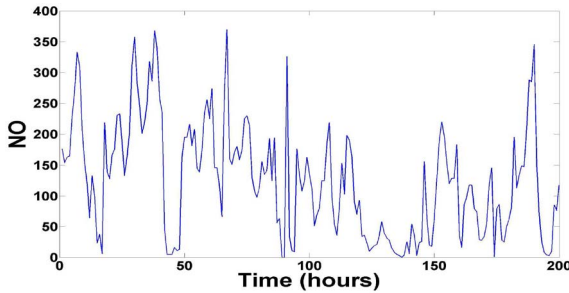


Fig. 7. Typical behavior of NO concentrations at a node as a function of time. The behavior of NO<sub>2</sub> is similar.

In this case, the coordinator can skip the tests of whether the pairs of nodes balance each other, and proceed to test whether all 4 nodes jointly can resolve the violation. If not, the coordinator asks for the local vectors of nodes  $N_2$ ,  $N_3$ ,  $N_6$  and  $N_8$ .

## 6 EXPERIMENTS

HGM was implemented and compared with the GM method, as described in [5], which is the most recent variant of previous work on geometric monitoring that we know of. We are not aware of other algorithms which can be applied to monitor the functions treated here (the ratio queries in [27] deal with accumulative ratios and not instantaneous ones as in our experiments).

### 6.1 Data, Setup and Monitored Functions

#### 6.1.1 Data and Monitored Functions

Our data consists of air pollutant measurements taken from “AirBase – The European Air Quality Database” [43], measured in micrograms per cubic meter. Nodes correspond to sensors at different geographical locations. The data at different nodes greatly varies in size and shape (see Section 6.2.2) and is irregular as a function of time, as shown in Fig. 7 (note however that we use the pdf of the data values per se, not as a time series). The quality of results was measured by the amount of reduction in communication, which is proportional to the number of safe-zone violations.

The monitored functions were chosen due to their practical importance, and also as they are non-linear and non-monotonic and, thus, cannot be handled by most existing methods. In Section 6.2 results are presented for monitoring the ratio of NO to NO<sub>2</sub>, which is known to be an important indicator in air quality analysis [44]. In Section 6.3 the chi-square distance between histograms was monitored for five-dimensional data. An example of monitoring a quadratic function in three variables is also presented (Section 6.4); quadratic functions are important in numerous applications (e.g., the variance is a quadratic function in the variables, and a normal distribution is the exponent of a quadratic function, hence thresholding it is equivalent to thresholding the quadratic).

#### 6.1.2 Choosing the Family of Safe-Zones

To solve the optimization problem, it is necessary to define a parametric family of shapes  $S$  from which the safe-zones

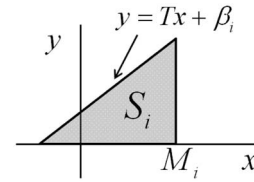


Fig. 8. Triangular safe-zones used for ratio monitoring.

will be chosen. Section 4.2 discusses the properties this family should satisfy. In [5], the suitability of some families of polytopes is studied for the simpler, but related, problem of finding a safe-zone common to all nodes. The motivations for choosing  $S$  here were:

- Ratio queries (Section 6.2) – the triangular safe-zones (Fig. 8) have the same structure, but not size or location, as  $C$ , and are very simple to define and apply.
- Chi-square monitoring (Section 6.3) – here the motivation was to choose safe-zones with a very simple shape, which still enabled a very substantial improvement over GM. We thus applied boxes (hyperrectangles), which are also attractive as they render the computation of the Minkowski average trivial.
- Quadratic function (Section 6.4) – here we allowed general polytopes, and tested the results for increasing numbers of vertices, using the Bayesian model selection paradigm (Section 4.2). The model selected was with 12 vertices.

Considering the complexity of the safe-zone problem, and the richness of the space of possible solutions, the challenge of choosing  $S$  for arbitrary functions and data distributions is quite formidable. The solutions provided here offer very good performance in terms of safe-zone simplicity and communication reduction over previous work, but the general problem deserves further study.

#### 6.1.3 Optimization Parameters and Tools

The triangular safe-zones (Section 6.2) have two degrees of freedom each ( $M_i$  and  $\beta_i$ , see Fig. 8), hence for  $n$  nodes we have  $2n$  parameters to optimize over. For the chi-square monitoring (Section 6.3), each safe-zone is a box in  $\mathcal{R}^5$  and therefore is defined by 10 parameters. The safe-zones in Section 6.4 require 36 parameters each. In all cases we used the Matlab routine `fmincon` to solve the optimization problem [45]. To compute the integral of the pdf on the safe-zones, data was approximated by a Gaussian Mixture Model (GMM), using a Matlab routine [46].

#### 6.1.4 Training/Testing Data, and Stability of the pdf Over Time

The proposed algorithm first learns the pdfs at the nodes, and then applies them in order to construct safe-zones. In order to assign safe-zones which will perform well over time, a probabilistic model of the pdfs is required, as in [5], [20]. In our experiments, we learned the model from the “Airbase” data [43] for every month in the year 2006 (training set), and used it to monitor the data for 2007-2008

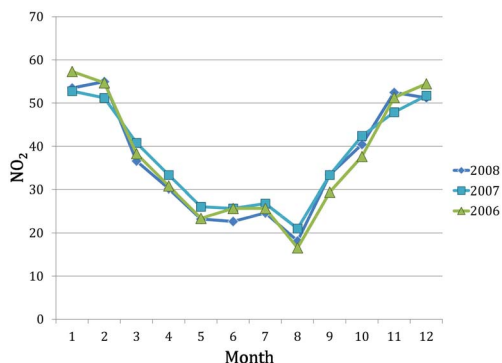


Fig. 9. Monthly  $\text{NO}_2$  concentrations over three years.

(testing set). As it can be seen in Fig. 9, the average concentration of  $\text{NO}_2$  was stable over these three years, and so was the  $\text{NO}$  concentration.

## 6.2 Ratio Queries

This set of experiments concerned monitoring the ratio between two pollutants,  $\text{NO}$  and  $\text{NO}_2$ , measured in distinct sensors. Each of the  $n$  nodes holds a vector  $(x_i, y_i)$  (the two concentrations), and the monitored function is  $\frac{\sum y_i}{\sum x_i}$  (in [27] ratio is monitored but over aggregates over time, while here we monitor the instantaneous ratio for the current readings). An alert must be sent whenever this function is above a threshold  $T$  (taken as 4 in the experiments), and/or when the  $\text{NO}_2$  concentration is above 250. The admissible region  $A$  is a triangle, therefore convex, so  $C = A$ . The safe-zones tested were triangles of the form depicted in Fig. 8, a choice motivated by the shape of  $C$ . The half-planes method (Section 4.4) was used to test the constraints. An example with four nodes, which demonstrates the advantage of allowing different safe-zones at the distinct nodes, is depicted in Fig. 10.

### 6.2.1 Improvement Over Previous GM Work

We compare HGM with GM in terms of the number of produced local violations. Unless specified otherwise, HGM always uses the hierarchical clustering algorithm for deriving the safe-zones at different nodes. In Fig. 11, the number of safe-zone violations is compared for various numbers of nodes. HGM results in significantly fewer local violations, even for a small number of nodes. As the number of nodes

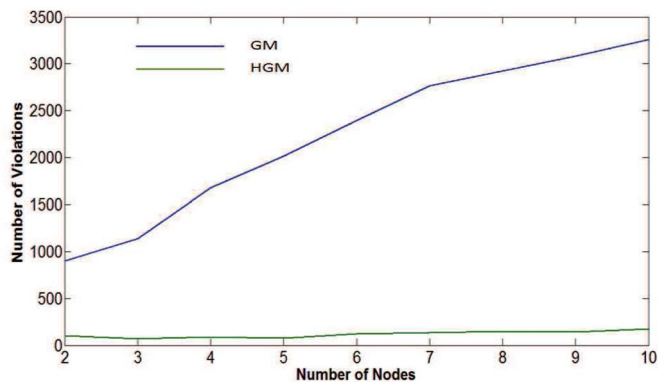


Fig. 11. Comparison of our HGM (green) to GM [5] (blue) in terms of number of violations, up to 10 nodes.

increases, the benefits of HGM over GM increase. For a modest network size of 10 nodes, HGM requires less than an order of magnitude fewer messages than GM. In Fig. 12 we compare some of the safe-zones that were obtained for both methods in this experiment.

### 6.2.2 Hierarchical Implementation for Ratio Queries

Hierarchical clustering of the nodes was applied in order to reduce the running time of the safe-zone computation. In Fig. 13 a typical result is depicted: 92 nodes were clustered into four groups. Two representatives from each of the three largest groups are shown, which correspond to three typical data types: “small” ones (left), indicating low concentrations of  $\text{NO}/\text{NO}_2$ , “drift” ones (middle), with many measurements near the origin but also a sizable number of measurements with high  $\text{NO}$  concentrations, and “vertical” ones (right), where most measurements are concentrated in a vertical stripe near the origin and there are fewer measurements with high  $\text{NO}$ . The Matlab routine `kmeans` [47] was used for clustering the moment vectors.

In order to test running time and performance, we ran the ratio monitoring algorithm for  $n = 30$  to 240 nodes with various thresholds, using either a “flat” mode (direct optimization over  $2n$  variables) or the hierarchical clustering method. Table 2 summarizes the results for  $n = 60$  and various values of the threshold  $T$ , where in each table entry the first number stands for running time (seconds) and the second number for the value of the target function (TF).

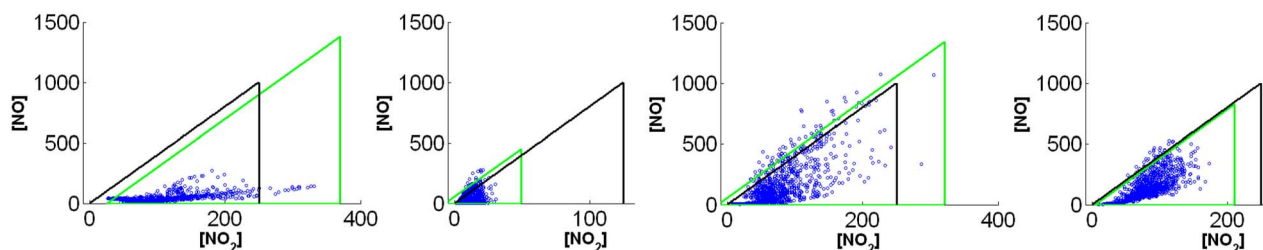


Fig. 10. Example of safe-zones with four nodes. The convex set  $C$  is the triangle outlined in black, safe-zones are outlined in green. Nodes with more compact distributions are assigned smaller safe-zones, and nodes with high values of the monitored function ( $\text{NO}/\text{NO}_2$  ratio) are assigned safe-zones which are translated to the left in order to cover more data. This is especially evident in the second from left node, in which the safe-zone is shifted to the left so it can cover almost all the data points. In order to satisfy the Minkowski sum constraint, the safe-zone of the first from left node is shifted to the right, which in that node hardly sacrifices any data points; also, the larger safe-zones are balanced by the smaller ones. Note that HGM allows safe-zones which are *larger* than the admissible region  $A$ , as opposed to previous work, in which the safe-zones are subsets of  $A$ .

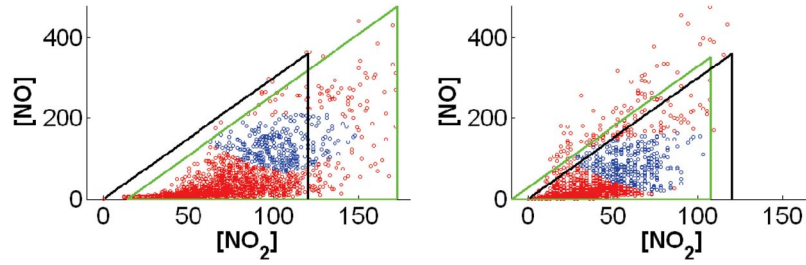


Fig. 12. Comparison of HGM to GM in terms of points which cause a violation. At each node, the set  $C$  is depicted (dark triangle), the safe-zones of HGM (green triangles), and a sample of the data points (red dots). The points which satisfy the GM constraints are depicted in blue. The advantage of HGM is clear.

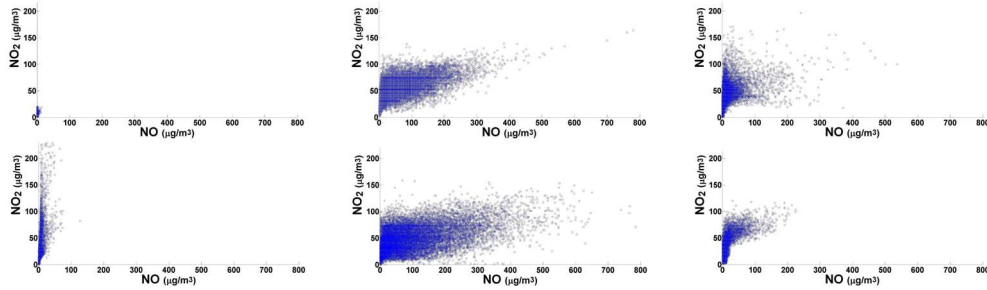


Fig. 13. Clustering example. Each column depicts two nodes from one clusters.

TABLE 2  
Optimization Time and Target Function (TF) for Ratio Queries, Varying the Threshold  $T$

	$T = 4$		$T = 3$		$T = 2$	
	Time	TF	Time	TF	Time	TF
Tree	23.9 secs.	0.980	23.4 secs.	0.985	23.8 secs.	0.962
Flat	243.6 secs.	0.999	244.9 secs.	0.994	177.4 secs.	0.970

TABLE 3  
Optimization Time Breakdown

	$T = 4$		$T = 3$		$T = 2$	
	Optimization	Other	Optimization	Other	Optimization	Other
Tree	54.2%	45.8%	53.0%	47.0%	56.1%	43.9%
Flat	96.2%	3.8%	96.1%	3.9%	95.5%	4.5%

The running time is higher for the “flat” mode, as the number of parameters to optimize over is much higher, but the performance is slightly better. Table 3 details the breakdown of the entire process, with “optimization” standing for the non-linear optimization, and “other” for computing the nodes’ moments and clustering. In Fig. 14 we plot the running time of “flat” vs. “hierarchical” as we vary the number of nodes. The running time for “hierarchical” increases linearly with the number of nodes. For 240 nodes, “hierarchical” results in a 40-fold reduction over “flat”.

### 6.3 Chi-Square Monitoring

Another example of an important non-linear, non-monotonic function is the chi-square distance between two histograms, defined by  $\chi(f, g) = \sum \frac{(f_i - g_i)^2}{f_i + g_i}$  for histograms  $f, g$ . Each histogram was defined as the concentration

levels of five pollutants and the monitored function was the chi-square distance between the hourly average of two nodes and their average calculated over the previous week (i.e., a measure of how much the hourly distribution deviates from last week’s average). The set  $C$  was defined as in [5]. The family of safe-zones consisted of five dimensional axis-aligned boxes. An exact solution for box safe-zones is NP-hard even for one-dimensional data (Section 7); so, as in the other experiments, an optimization toolbox was used (Section 6.1.3). When the data distributions in two nodes substantially differ, the advantage of HGM over GM is very clear, since HGM can adapt its safe-zones to fit the distinct distributions at the nodes, allowing a much larger safe-zone to the node with the more varying data. In Figs. 15 and 16 the different behavior between the nodes is demonstrated and the safe-zones allocated to them is depicted. In Fig. 17 we plot the ratio

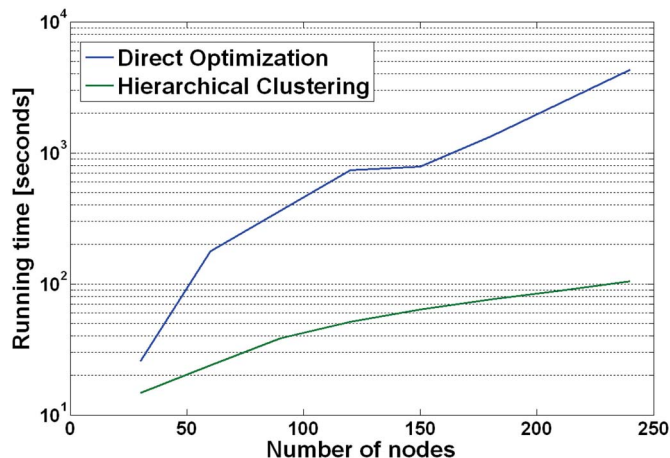


Fig. 14. Running time (in logarithmic scale) for “flat”/direct optimization over all the nodes (blue) vs. hierarchical clustering (green).

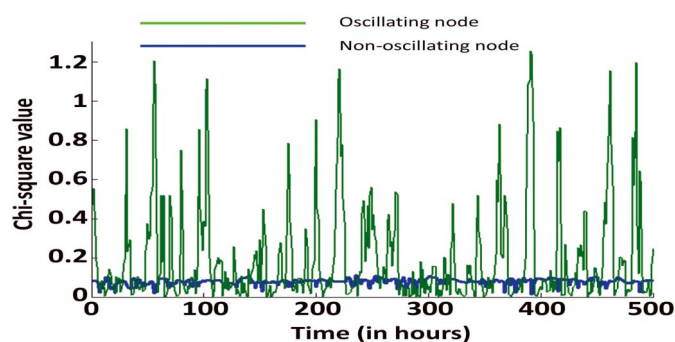


Fig. 15. Plots of the chi-square function for two nodes, an “oscillating” one (highly varying data) in green, and a more stable node (in blue).

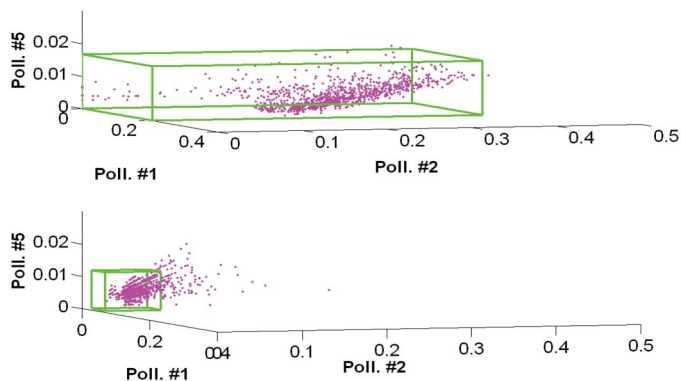


Fig. 16. Safe-zones assigned to the two nodes in Fig. 15. The “oscillating” node (top) is assigned a much larger safe-zone, to account for its higher variability. The data is five-dimensional, and a three-dimensional projection is depicted, corresponding to the pollutants NO, NO<sub>2</sub>, and SO<sub>2</sub>. Pink dots denote samples from the data, safe-zones are in green.

of violations of GM over HGM for various thresholds, for a period of 1,000 hours. As the threshold increases, HGM becomes more superior. For the low thresholds, 0.5 to 0.6, there are actual (global) violations, but as the threshold increases, GM suffers from many “false alarms” (local violations which do not indicate a global violation), but HGM performs well.

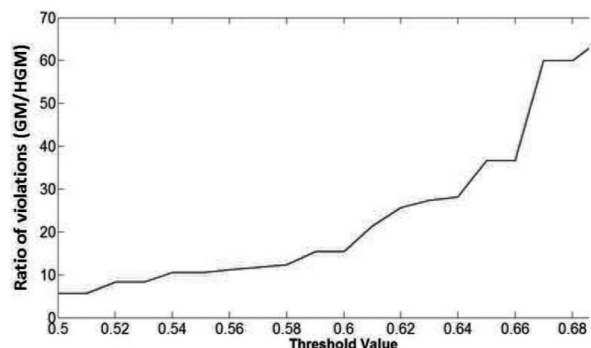


Fig. 17. Comparing the number of GM vs. HGM violations. Horizontal axis is the threshold  $T$  for the chi-square function, vertical axis is the ratio between numbers of violations in GM vs. HGM.

## 6.4 Monitoring a Quadratic Function

Another example consists of monitoring a quadratic function with more general polyhedral safe-zones in three variables (Fig. 18). The data consists of measurements of three pollutants (NO, NO<sub>2</sub>, SO<sub>2</sub>), and the safe-zones are polyhedra with 12 vertices, where the number of vertices was chosen according to the Bayesian model selection paradigm (Section 4.2). In Fig. 19, the model evidence (Lemma 1) is plotted as a function of the number of safe-zone vertices (since the dimension is three, the minimal number of vertices is four). The admissible region  $A$  is the ellipsoid depicted in pink; since it is convex,  $C = A$ . As the extent of the data is far larger than  $A$ , the safe-zones surround the regions in which the data is denser. In order to check the constraints, the direct method was applied (Section 4.4), with the implicit quadratic function defining the ellipsoid. For this experiment, the running time for computing the safe-zones was on the average 7.9 seconds for a pair of nodes, and the reduction in communication relative to GM was by a factor of 78.4%.

## 6.5 Violation Recovery Performance

We tested the violation recovery algorithm (Section 5) for ratio monitoring (Section 6.2). We randomly chose 64 nodes, over 10,000 hourly measurements. On average, the recovery algorithm enabled 61% of the local violations to be resolved between pairs (Type 2 nodes), 23% required Type 4 nodes, 10% required Type 8 nodes, 3% required Type 16 nodes, 2% required Type 32 nodes, and only 1% required collecting data from all 64 nodes. Thus, on the average, only 4.7 nodes out of 64 were required to resolve a violation.

## 7 COMPLEXITY OF THE SAFE-ZONE PROBLEM

We next state three theorems which concern the complexity of the safe-zone assignment problem, as formulated in Section 3. Due to lack of space, we cannot include the proofs; they appear in <http://www.cs.haifa.ac.il/~dkeren/mypapers/long-TKDE-2014.pdf>

**Theorem 1.** *The safe-zone problem, even for two nodes and one-dimensional data, is NP-hard and inapproximable.*

One may suspect that the difficulty of the safe-zone problem is due to allowing a discrete, disconnected admissible region as above. The following theorems prove that is not the case.

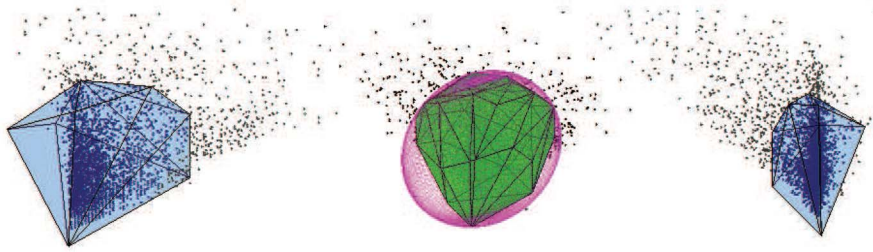


Fig. 18. Monitoring a quadratic function. The set  $C$  is the pink ellipsoid, the safe-zones are polyhedra with 12 vertices each (in pale blue), and their Minkowski average is in green.

**Theorem 2.** *If the dimension of the data vectors is at least 4, the optimal safe-zone problem is NP-complete for two nodes even when  $A$  is convex.*

**Theorem 3.** *For more than two nodes, the safe-zone problem is NP-Complete when  $A$  is a one-dimensional interval.*

## 8 CONCLUSION

A method for monitoring threshold queries over heterogeneous distributed streams was presented. A paradigm for minimizing communication is formulated as an optimization problem of a geometric and probabilistic flavor, whose solution assigns each node a “safe-zone” with the property that a node may remain silent as long as its data vector is in its safe-zone. While the problem is shown to be difficult, a practical solution using a hierarchical clustering algorithm is presented and implemented for two, three, and five dimensional data, allowing to achieve substantial improvement over previous work, while using rather simple safe-zones which also reduce the computational effort at the nodes.

## REFERENCES

- [1] D. J. Abadi *et al.*, “The design of the borealis stream processing engine,” in *Proc. CIDR*, Asilomar, CA, USA, 2005.
- [2] I. Sharfman, A. Schuster, and D. Keren, “A geometric approach to monitoring threshold functions over distributed data streams,” *ACM Trans. Database Syst.*, vol. 32, no. 4, Article 23, Nov. 2007.
- [3] S. Burdakis and A. Deligiannakis, “Detecting outliers in sensor networks using the geometric approach,” in *Proc. ICDE*, Washington, DC, USA, 2012, pp. 1108–1119.
- [4] N. Giatrakis, A. Deligiannakis, M. N. Garofalakis, I. Sharfman, and A. Schuster, “Prediction-based geometric monitoring over distributed data streams,” in *Proc. SIGMOD*, Scottsdale, AZ, USA, 2012.
- [5] D. Keren, I. Sharfman, A. Schuster, and A. Livne, “Shape sensitive geometric monitoring,” *IEEE Trans. Knowl. Data Eng.*, vol. 24, no. 8, pp. 1520–1535, Aug. 2012.

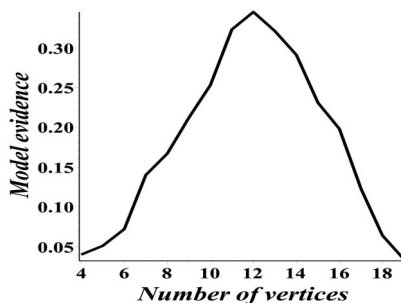


Fig. 19. Evidence for modeling safe-zones for the data in Fig. 18 as a function of the number of vertices.

- [6] G. Sagy, D. Keren, I. Sharfman, and A. Schuster, “Distributed threshold querying of general functions by a difference of monotonic representation,” *Proc. VLDB*, vol. 4, no. 2, pp. 46–57, Nov. 2010.
- [7] G. Cormode and M. N. Garofalakis, “Sketching streams through the net: Distributed approximate query tracking,” in *Proc. VLDB*, Trondheim, Norway, 2005, pp. 13–24.
- [8] L. Huang *et al.*, “Communication-efficient online detection of network-wide anomalies,” in *Proc. INFOCOM*, Anchorage, AK, USA, 2007, pp. 134–142.
- [9] A. Arasu and G. S. Manku, “Approximate counts and quantiles over sliding windows,” in *Proc. PODS*, Paris, France, 2004, pp. 286–296.
- [10] G. Cormode and M. N. Garofalakis, “Histograms and wavelets on probabilistic data,” in *Proc. ICDE*, 2009.
- [11] A. Manjhi, V. Shkapenyuk, K. Dhamdhere, and C. Olston, “Finding (recently) frequent items in distributed data streams,” in *Proc. ICDE*, Washington, DC, USA, 2005, pp. 767–778.
- [12] K. Yi and Q. Zhang, “Optimal tracking of distributed heavy hitters and quantiles,” in *Proc. PODS*, Providence, RI, USA, 2009.
- [13] G. Cormode, M. N. Garofalakis, S. Muthukrishnan, and R. Rastogi, “Holistic aggregates in a networked world: Distributed tracking of approximate quantiles,” in *Proc. SIGMOD*, Baltimore, MD, USA, 2005.
- [14] G. Cormode, S. Muthukrishnan, and W. Zhuang, “What’s different: Distributed, continuous monitoring of duplicate-resilient aggregates on data streams,” in *Proc. ICDE*, Washington, DC, USA, 2006, p. 57.
- [15] G. Cormode, S. Muthukrishnan, K. Yi, and Q. Zhang, “Optimal sampling from distributed streams,” in *Proc. PODS*, Indianapolis, IN, USA, 2010.
- [16] A. Bar-Or, D. Keren, A. Schuster, and R. Wolff, “Hierarchical decision tree induction in distributed genomic databases,” *IEEE Trans. Knowl. Data Eng.*, vol. 17, no. 8, pp. 1138–1151, Aug. 2005.
- [17] F. Li, K. Yi, and J. Jester, “Ranking distributed probabilistic data,” in *Proc. SIGMOD*, Providence, RI, USA, 2009.
- [18] G. Cormode, S. Muthukrishnan, and K. Yi, “Algorithms for distributed functional monitoring,” in *Proc. SODA*, Philadelphia, PA, USA, 2008.
- [19] C. Arackaparambil, J. Brody, and A. Chakrabarti, “Functional monitoring without monotonicity,” in *Proc. ICALP*, Rhodes, Greece, 2009.
- [20] A. Deshpande, C. Guestrin, S. Madden, J. M. Hellerstein, and W. Hong, “Model-driven data acquisition in sensor networks,” in *Proc. VLDB*, Toronto, ON, Canada, 2004.
- [21] M. Tang, F. Li, J. M. Phillips, and J. Jester, “Efficient threshold monitoring for distributed probabilistic data,” in *Proc. ICDE*, Washington, DC, USA, 2012, pp. 1120–1131.
- [22] R. Keralapura, G. Cormode, and J. Ramamirtham, “Communication-efficient distributed monitoring of thresholded counts,” in *Proc. SIGMOD*, Chicago, IL, USA, 2006.
- [23] D. P. Woodruff and Q. Zhang, “Tight bounds for distributed functional monitoring,” in *Proc. STOC*, 2012, pp. 941–960.
- [24] R. Wolff, K. Bhaduri, and H. Kargupta, “A generic local algorithm for mining data streams in large distributed systems,” *IEEE Trans. Knowl. Data Eng.*, vol. 21, no. 4, pp. 465–478, Apr. 2009.
- [25] S. Shah and K. Ramamirtham, “Handling non-linear polynomial queries over dynamic data,” in *Proc. ICDE*, Cancun, Mexico, 2008.
- [26] S. Michel, P. Triantafillou, and G. Weikum, “KLEE: A framework for distributed top-k query algorithms,” in *Proc. VLDB*, 2005, pp. 637–648.

- [27] R. Gupta, K. Ramamritham, and M. K. Mohania, "Ratio threshold queries over distributed data sources," in *Proc. ICDE*, Long Beach, CA, USA, 2010, pp. 581–584.
- [28] I. Sharfman, A. Schuster, and D. Keren, "Shape sensitive geometric monitoring," in *Proc. PODS*, Vancouver, BC, Canada, 2008, pp. 1520–1535.
- [29] G. Cormode, "Algorithms for continuous distributed monitoring: A survey," in *Proc. AIMoDEP*, 2011, pp. 1–10.
- [30] J. Kogan, "Feature selection over distributed data streams through optimization," in *Proc. SDM*, 2012, pp. 475–484.
- [31] O. Papapetrou, M. N. Garofalakis, and A. Deligiannakis, "Sketch-based querying of distributed sliding-window data streams," in *Proc. VLDB*, vol. 5, no. 10, pp. 992–1003, Jun. 2012.
- [32] M. N. Garofalakis, D. Keren, and V. Samoladas, "Sketch-based geometric monitoring of distributed stream queries," in *Proc. VLDB*, vol. 6, no. 10, pp. 937–948, Aug. 2013.
- [33] B. Kanagal and A. Deshpande, "Online filtering, smoothing and probabilistic modeling of streaming data," in *Proc. ICDE*, Cancun, Mexico, Apr. 2008, pp. 1160–1169.
- [34] J. Serra, *Image Analysis and Mathematical Morphology*. Orlando, FL, USA: Academic Press, 1982.
- [35] B. Wirth, L. Bar, M. Rumpf, and G. Sapiro, "A continuum mechanical approach to geodesics in shape space," *Int. J. Comput. Vis.*, vol. 93, no. 3, pp. 293–318, Jul. 2011.
- [36] D. Keren, D. B. Cooper, and J. Subrahmonia, "Describing complicated objects by implicit polynomials," *IEEE Trans. Pattern Anal. Mach. Intell.*, vol. 16, no. 1, pp. 38–53, Jan. 1994.
- [37] D. Mackay, "Bayesian interpolation," *Neural Comput.*, vol. 4, no. 3, pp. 415–447, May 1992.
- [38] J. Subrahmonia, D. B. Cooper, and D. Keren, "Practical reliable Bayesian recognition of 2D and 3D objects using implicit polynomials and algebraic invariants," *IEEE Trans. Pattern Anal. Mach. Intell.*, vol. 18, no. 5, pp. 505–519, May 1996.
- [39] H. R. Tiwary, "On the hardness of Minkowski addition and related operations," in *Proc. Symp. Computational Geometry*, New York, NY, USA, 2007, pp. 306–309.
- [40] Y. Gordon, M. Meyer, and S. Reisner, "Constructing a polytope to approximate a convex body," *Geometriae Dedicata*, vol. 57, no. 2, pp. 217–222, Sept. 1995.
- [41] E. Fogel and D. Halperin, "Exact and efficient construction of Minkowski sums of convex polyhedra with applications," *Computer-Aided Design*, vol. 39, no. 11, pp. 3–15, 2007.
- [42] M. Elad, A. Tal, and S. Ar, "Content based retrieval of VRML objects: An iterative and interactive approach," in *Proc. Multimedia 2001*, New York, NY, USA, 2002, pp. 107–118.
- [43] *The European Air Quality Database* [Online]. Available: <http://tinyurl.com/ct9bh7x>
- [44] M. Kurpius and A. Goldstein, "Gas-phase chemistry dominates O<sub>3</sub> loss to a forest, implying a source of aerosols and hydroxyl radicals to the atmosphere," *Geophys. Res. Lett.*, vol. 30, no. 7, pp. 24.1–24.4, 2003.
- [45] [Online]. Available: <http://tinyurl.com/kxssfj>
- [46] *DCPR (Data Clustering and Pattern Recognition) Toolbox* [Online]. Available: <http://tinyurl.com/nxospq2>
- [47] [Online]. Available: <http://www.mathworks.com/help/toolbox/stats/kmeans.html>

**Daniel Keren** (Ph.D. 1991, Hebrew University in Jerusalem) is with the Computer Science Department in Haifa University, Haifa, Israel. Since 2003, he has been working closely with Prof. Assaf Schuster's group at the Technion, in the area of distributed monitoring. His other interests include computer vision, machine learning, and regularization.

**Guy Sagy** completed his Ph.D. degree at the Computer Science Faculty, the Technion, in 2011. His main areas of research are distributed algorithms and geometric methods for stream processing.

**Izchak Sharfman** completed his Ph.D. degree at the Computer Science Faculty, the Technion, in 2008. His main areas of research are distributed algorithms and geometric methods for stream processing. He is currently a post-doctoral researcher in the Technion.

**Amir Abboud** graduated with a B.Sc. degree from the "Etgar" program at Haifa University, completed his M.Sc. degree at the Technion, and is currently a Ph.D. student at Stanford University.



**David Ben-David** graduated with a M.Sc. degree from the Computer Science Faculty in the Technion, 2012. His work concerned distributed monitoring. He is currently a software engineer at EMC, Israel.



**Assaf Schuster** has established and is managing DSL, the Distributed Systems Laboratory (<http://dsl.cs.technion.ac.il>). Prof. Schuster is well known in the area of parallel, distributed, high performance, and grid computing. He published over 160 papers in these areas in high-quality conferences and journals. He consults the hi-tech industry on related issues and holds seven patents. He serves as an associate editor of the *Journal of Parallel and Distributed Computing*, and *IEEE Transactions on Computers*.



**Antonios Deligiannakis** is an Assistant Professor of Computer Science in the Dept. of Electronic & Computer Engineering of the Technical Univ. of Crete, as of January 2008. He received the Diploma degree in Electrical and Computer Engineering from the National Technical Univ. of Athens in 1999, and the MSc and PhD degrees in Computer Science from the Univ. of Maryland in 2001 and 2005, respectively. He then performed his PostDoctoral research in the Dept. of Informatics and Telecommunications at the Univ. of Athens (2006-2007). Prof. Deligiannakis is also an adjunct researcher at the Digital Curation Unit (<http://www.dcu.gr/>) of the IMIS-Athena Research Centre.

▷ For more information on this or any other computing topic, please visit our Digital Library at [www.computer.org/publications/dlib](http://www.computer.org/publications/dlib).